Electronic Supplementary Material (ESI) for Chemical Science.

Supporting Information

Designed Alpha-Helical Barrels for Charge-Selective Peptide Translocation

Smrithi Krishnan R[1,2†], Neethu Puthumadathil[1,2†], Amina H Shaji[1], K Santhosh Kumar[1], Gayathri Mohan[1] and Kozhinjampara R Mahendran[1]*

[†]Contributed equally to this work

[1]Membrane Biology Laboratory, Transdisciplinary Research Program, Rajiv Gandhi Centre for Biotechnology, Thiruvananthapuram 695014, India.

[2]Manipal Academy of Higher Education, Manipal, Karnataka, India-576104

*To whom correspondence should be addressed

*e-mail: mahendran@rgcb.res.in

Table of Contents

Materials and Supporting Text 3

Molecular dynamics simulations and molecular models of pPorA 3

SDS PAGE gel extraction of peptides 3

Supporting Table 5

Table S1: Hexaarginine binding kinetics 5

Table S2: Nonaarginine binding kinetics 6

Supporting Figures

Fig. S1: HPLC traces and MALDI-TOF MS for pPorA peptides 7

Fig. S2: Electrical properties of gpPorA 8

Fig. S3: The molecular models of pPorA and molecular dynamics simulations 9

Fig. S4: Interaction of tetraarginine with gpPorA 10

Fig. S5: Interaction of tetraarginine with gpPorA 11

Fig. S6: Interaction of hexaarginine with the cis side of gpPorA 12

Fig. S7: Interaction of hexaarginine with the trans side of gpPorA 13

Fig. S8: Interaction of nonaarginine with the cis side of gpPorA 14

Fig. S9: Interaction of nonaarginine with the trans side of gpPorA 15

Fig. S10: Interaction of nonaarginine with the cis and trans side of gpPorA 17

Fig. S11: Interaction of tetraarginine and nonaarginine with gpPorA 18

Fig. S12: Interaction of nonaarginine with gpPorA in 1 M KCl buffer 19

Fig. S13: pH-dependent interaction of nonaarginine with gpPorA 20

Fig. S14: Interaction of nonaspartate and nonaarginine with gpPorA 21

Fig. S15: Interaction of hexaarginine and nonaarginine with pPorA-K24 22

Fig. S16: Interaction of nonaarginine with pPorA-A24 23

Fig. S17: Interaction of hexaarginine with directly added pPorA peptides 24

Fig. S18: Interaction of nonaarginine with directly added pPorA peptides 25

References 26

Materials and Supporting Text:

The following materials were used for the study: 1,2-diphytanoyl-*sn*-glycero-3-phosphocholine (DPhPC, Avanti Polar Lipids), pentane (Sigma-Aldrich Merck), hexadecane (Sigma-Aldrich Merck), n-dodecyl β-D-maltoside (DDM, Sigma-Aldrich Merck), potassium chloride (Sigma-Aldrich Merck), 4-(2-hydroxyethyl)-1-piperazineethanesulfonic acid (HEPES, Sigma-Aldrich Merck), ethylenediaminetetraacetic acid disodium salt (EDTA, Sigma-Aldrich Merck), dithiothreitol (DTT, Sigma-Aldrich Merck), sodium chloride (Sigma-Aldrich Merck), 2-Propanol (Sigma-Aldrich Merck), Acetone(Sigma-Aldrich Merck), all other reagents (Sigma-Aldrich Merck). 2x Laemmli sample buffer (Bio-Rad), Any kD™ Mini-PROTEAN® TGX™ precast gel (Bio-Rad), Precision Plus Protein™ Dual Color Standards (Bio-Rad), All pPorA peptides and arginine peptides were purchased from Peptide Protein Research Ltd at >95% purity (HPLC) as lyophilized powders.

The molecular models of pPorA and molecular dynamics simulations:

The structure of pPorA is based on the modeled structure of natural porins PorACj.[1] We used this modeled structure of the PorACj in our schematic model figures representing the pPorA. In agreement with the experimental data, pPorA-C24 is proposed to form an octameric pore.[2] The modeled structures of pPorA are created using Pymol (The PYMOL Molecular Graphics System, version 2.3.2, Schrödinger, LLC) in Windows. In fig. 1e, fig. 2-4, fig. 5c and fig. S10, the models (deep purple) are shown in surface representation with negatively charged residues in red and positively charged residues in blue. In Fig. 6a (pPorA-K24) and 6b (pPorA-A24), the hexameric pore (Forest) is shown in surface representation with negatively charged residues in red, positively charged residues in marine.

Hexameric and octameric pore models were encased in cell-realistic membrane models via the online Charmm-GUI service.[3] The membrane bilayer was comprised of POPC, POPE and POPG lipids in a 3:1:1 ratio. For the hexameric pore, a total of 51 POPC, 17 POPE and 17 POPG molecules were included in both the upper and lower lipid layers. In the octameric pore, 48 POPC, 16 POPE and 16 POPG molecules were included in both the upper and lower lipid layers. In both cases, the lipids were packed to achieve a dense box that was roughly square in the X and Y coordinates, whereby the Z-axis aligns with the length of the pore channel. The resulting box was capped by a water buffer amounting to 15.0 Angstroms, both above and below the membrane. Neutralizing ions (hexamer: 27 Cl^- and 61 K^+; octamer: 28 Cl^- and 68 K^+) were interspersed within the solvent via Monte Carlo sampling (also performed by the Charmm-GUI). Forces and charges for all components in these simulations were represented

using the Charmm 3.6 force field.[4] The resulting structures were equilibrated in NAMD [5] at 303.15K, with Langevin piston optimizing the cell to achieve a stable density corresponding to 1.0-atmosphere pressure. Structural relaxation was accomplished during these equilibration simulations by gradual phasing out initial protein positional soft-restraints. Specifically, the first phase entailed 10,000 molecular mechanics optimization steps followed by 12,500 dynamic steps (2.0 ns per step) with a K=10.0 positional restraint on peptide atom positions. This simulation protocol was then repeated with a reduced value of K=5.0, followed subsequent phases (same number of mechanics and dynamics steps in all cases) with incremental values of K = 2.5, 1.0, and 0.5. A final pressure equilibration phase entailed 25,000 dynamics steps with K=0.1. For analysis, Gaussian Accelerated Molecular Dynamics simulations were performed.[6] A brief (40,000 steps) equilibration was performed at constant pressure (as sustained by Langevin piston) to alleviate any strains potentially arising from the switch from conventional dynamic forces to hyperdynamic potentials. This was followed by a 1,000,000 step production run. From a sample set of 100 evenly distributed trajectory snapshots, the charged surface exposure for both the hexameric and octameric pores were approximated by computing the individual atomic solvent-exposed cationic surface areas for each of the charged protons on the charged ammonium of each lysine. For anionic exposure, the same analysis was performed for each carboxylate oxygens on every aspartate and glutamate residue. In all cases, the solvent exposures were computed via the 'get_area' function within PyMol 2.5.

SDS PAGE gel extraction of peptides:

SDS-polyacrylamide gel electrophoresis (SDS-PAGE) was used to examine the oligomerization of DDM solubilized mutant pPorA peptides.[2, 7] The purified peptides solubilized in phosphate buffer containing 0.1% DDM were loaded on a Mini-PROTEAN® TGX™ precast gel (Bio-Rad) with Protein Standard Marker (Bio-Rad) followed by SDS PAGE. The electrophoretic mobility of peptides in SDS-PAGE was determined, and molecular mass was calculated based on denatured protein standards. Bands containing corresponding peptide oligomers were cut from the gel, and each gel slice was solubilized with 10 mM phosphate buffer (K_2HPO_4, KH_2PO_4, pH 7.4, 500 µL) and crushed with a plastic pestle and cut into tiny pieces. After 45 min at room temperature, the gel fragments were removed with microfilterfuge tubes by centrifugation at 15,000 xg. Finally, the filtrate containing the peptide oligomers was used to test the pore-forming activity in the single-channel electrical recordings.

Supporting Table 1

Hexaarginine added to the cis side in 150mM KCl			
Voltage [mV]	**k_{on} [$M^{-1}s^{-1}$]** x 10^7	**k_{off} [s^{-1}]**	**K_D [k_{off}/k_{on}] [M]** x 10^{-7}
-5	35.04 ± 4	1000 ± 108	28.53 ± 3
-10	32.09 ± 3	1666.66 ± 160	51.93 ± 5
-15	26.02 ± 3	2500.25 ± 250	96.08 ± 10
-20	18.5 ± 2	3448.27 ± 340	186.39 ± 20
-25	15.42 ± 2	4545.45 ± 450	294.77 ± 30
Hexaarginine added to the trans side in 150mM KCl			
Voltage [mV]	**k_{on} [$M^{-1}s^{-1}$]** x 10^7	**k_{off} [s^{-1}]**	**K_D [k_{off}/k_{on}] [M]** x 10^{-7}
+5	33.32 ± 3.5	1086.95 ± 100	32.62 ± 3
+10	29.14 ± 3	1428.57 ± 140	49.02 ± 5
+15	23.32 ± 2.5	2300.5 ± 250	98.64 ± 10
+20	17.07 ± 2	3333.33 ± 340	195.27 ± 20
+25	15.32 ± 2	4347.82 ± 430	283.80 ± 30

Table S1: Hexaarginine binding kinetics.

The dissociation constants ($K_D = k_{off}/k_{on}$) were calculated from the association (k_{on}) and dissociation (k_{off}) rate constants. Electrolyte: 150 mM KCl, 10 mM HEPES, pH 7.4. Hexaarginine was added to the cis side and trans side. Mean values (± s.d.) from at least three independent experiments (n = 3) are shown.

Nonaarginine added to the cis side in 150mM KCl			
Voltage [mV]	**k_{on} [$M^{-1}s^{-1}$]** x 10^7	**k_{off} [s^{-1}]**	**K_D [k_{off}/k_{on}] [M]** x 10^{-7}
-5	Pore closed	Pore closed	Pore closed
-10	1.2 ± 0.1	11.11 ± 1	9.26 ± 1
-15	6 ± 0.6	66.66 ± 7	11.11 ± 1
-20	14.46 ± 1.5	196.07 ± 20	13.56 ± 1.5
-25	28.53 ± 3	526.31 ± 53	18.44 ± 2
-30	40 ± 4	1111.11 ± 111	27.77 ± 3
-35	42 ± 4	2857.14 ± 290	68.02 ± 7
-40	30 ± 3	5000 ± 500	166.66 ± 20
Nonaarginine added to the trans side in 150mM KCl			
Voltage [mV]	**k_{on} [$M^{-1}s^{-1}$]** x 10^7	**k_{off} [s^{-1}]**	**K_D [k_{off}/k_{on}] [M]** x 10^{-7}
+5	0.97 ± 0.1	11.76 ± 2	12.08 ± 1
+10	2.80 ± 0.3	28.57 ± 3	10.19 ± 1
+15	7 ± 0.7	100 ± 10	14.28 ± 1.5
+20	13 ± 1	256.41± 25	19.72 ± 2
+25	19.6 ± 2	606.06 ± 60	30.92 ± 3
+30	31.52 ± 3	1428.57 ± 150	45.30 ± 5
+35	38.44 ± 4	2702.70 ± 300	70.30 ± 7
+40	30 ± 3	5000 ± 500	166.66 ± 20

Table S2: Nonaarginine binding kinetics.

The dissociation constants (K_D = k_{off}/k_{on}) were calculated from the association (k_{on}) and dissociation (k_{off}) rate constants. Electrolyte: 150 mM KCl, 10 mM HEPES, pH 7.4. Nonaarginine was added to the cis side and trans side. Mean values (± s.d.) from at least three independent experiments (n = 3) are shown.

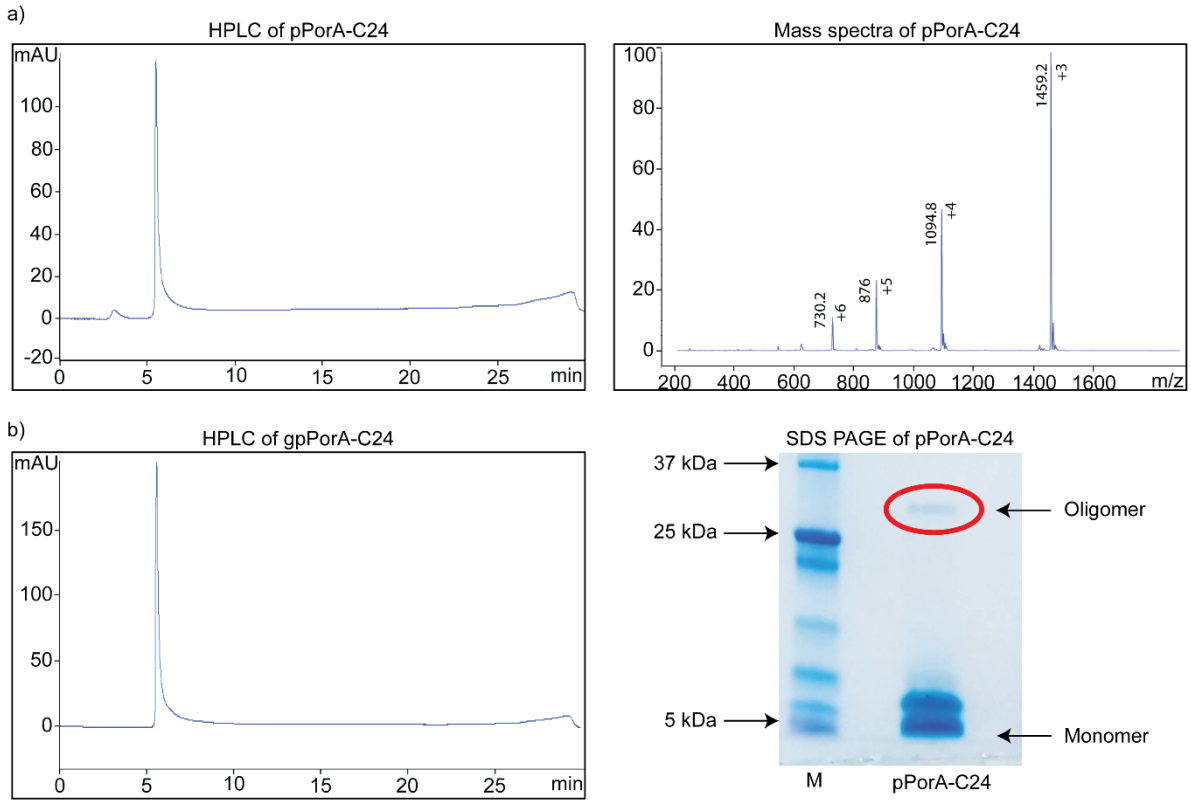

Fig. S1: HPLC traces and MALDI-TOF MS for pPorA peptides.

a) HPLC traces and MALDI-TOF MS for pPorA-C24 peptides. **b)** HPLC traces and the pPorA-C24 run on an SDS-PAGE showing gpPorA octamers.

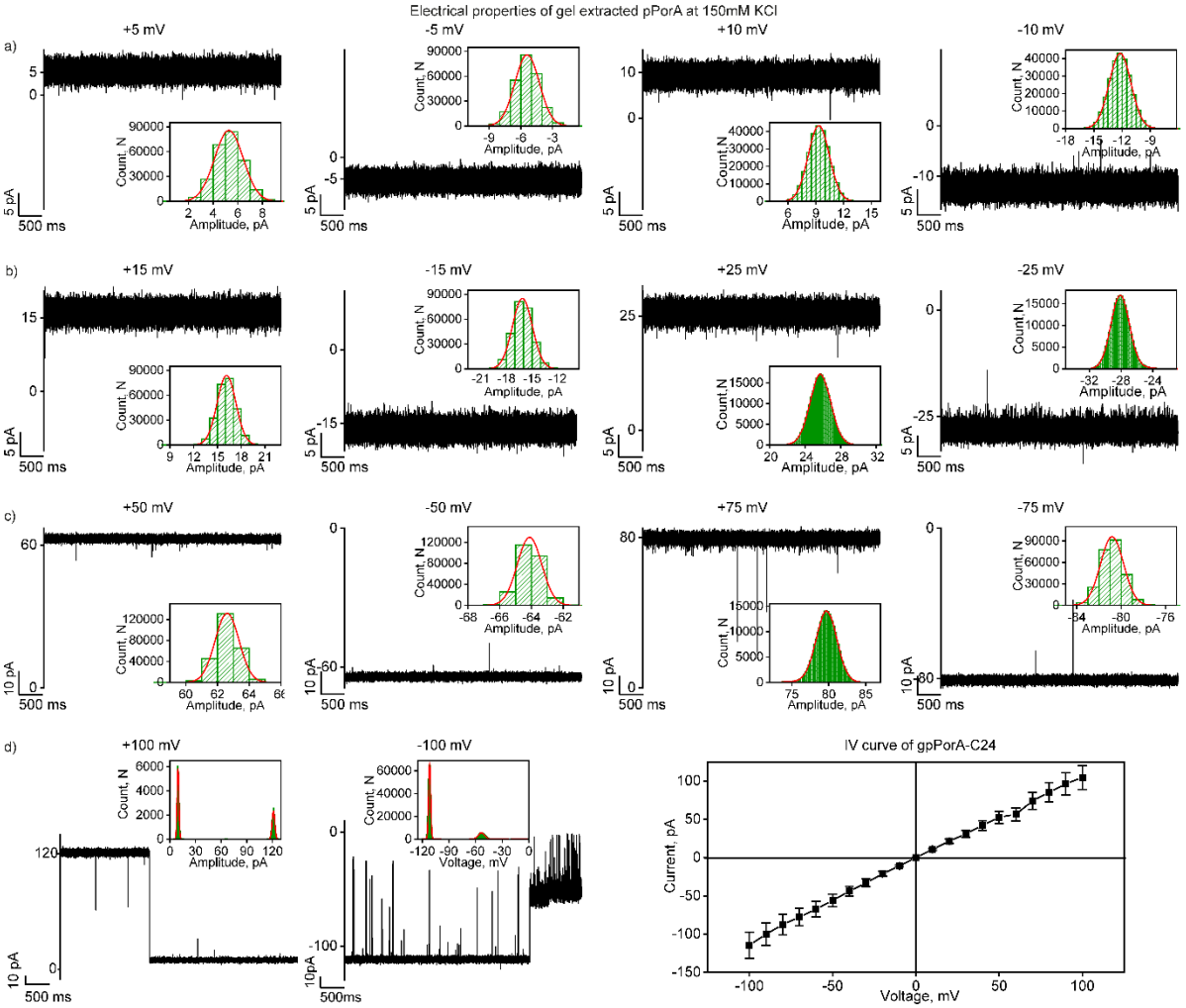

Fig. S2: Electrical properties of gpPorA

Electrical recording of gpPorA at **a**) ±5 mV and ± 10 mV, **b**) ± 15 mV and ± 25 mV **c**) ±50 mV and ± 75 mV and **d)** ±100 mV and I-V curve. The corresponding amplitude histogram is shown. Electrolyte: 150 mM KCl, 10 mM HEPES, pH 7.4. The current signals were filtered at 2 kHz and sampled at 10 kHz.

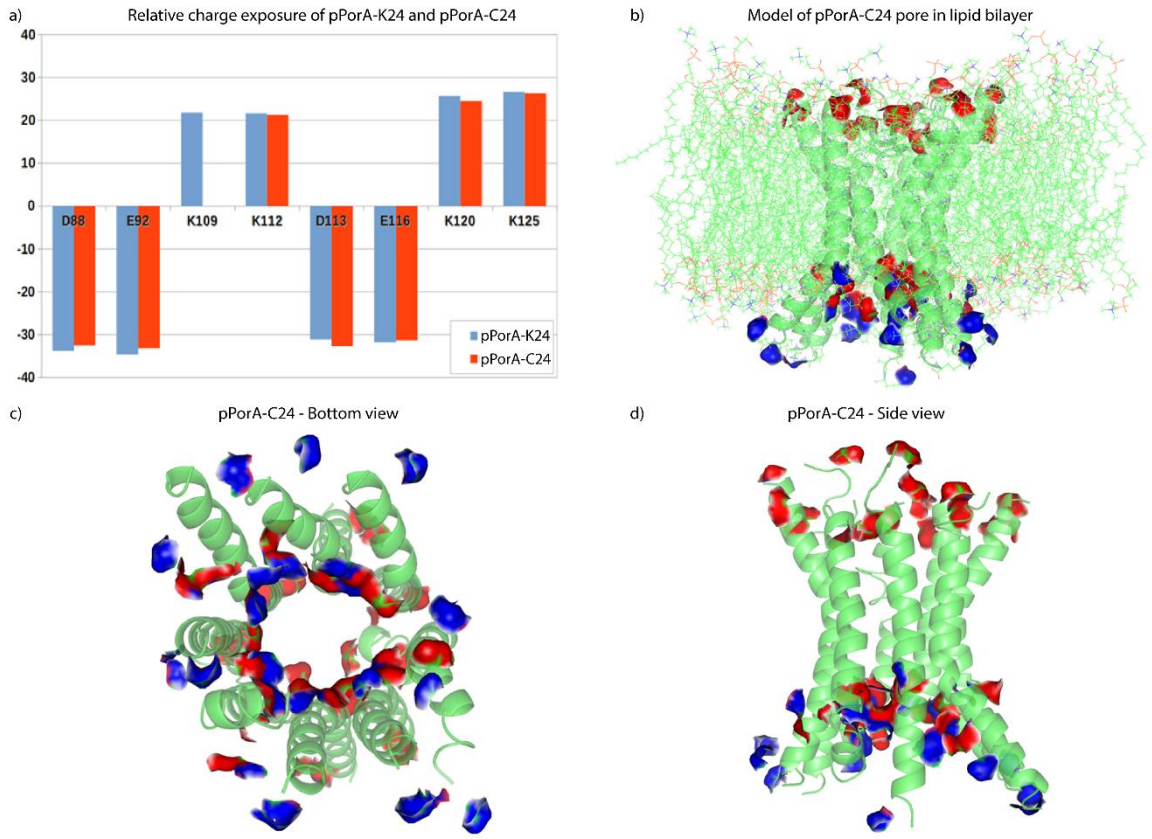

Fig. S3: Molecular dynamics simulations and modeled structure of pPorA

a) The bar chart showing hexamer charge exposure (pPorA-K24) and octamer charge exposure (pPorA-C24) for each charged residue (averaged over all monomers) in the hexamer and octamer structures**. b)** Modeled pPorA octamer structure in cartoon (side view) **c, d)** bottom view and side view. The cationic residues are shown in blue and anionic residues in red.

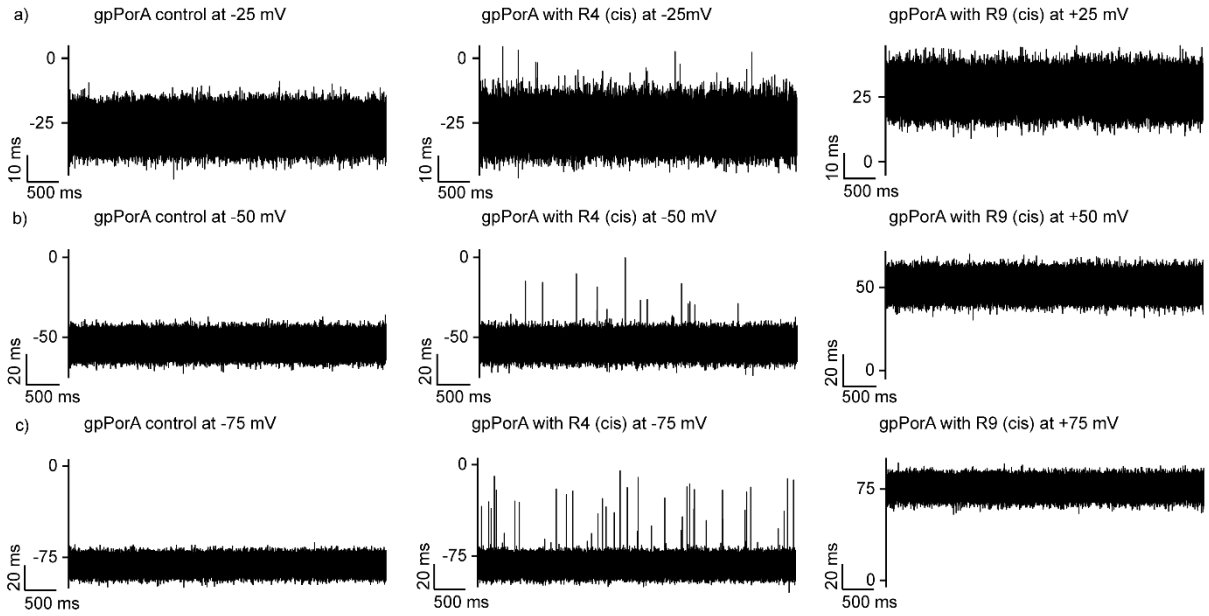

Fig. S4: Interaction of tetraarginine with gpPorA

a) Electrical recordings showing gpPorA at -25 mV and the interaction of tetraarginine (R4) with single gpPorA (10 µM, cis) at ±25. **b)** Electrical recordings showing gpPorA at -50 mV the interaction of R4 with single gpPorA (10 µM, cis) at ± 50 mV **c)** Electrical recordings showing gpPorA at -75 mV and the interaction of R4 with single gpPorA (10 µM, cis) at ±75. Electrolyte: 150 mM KCl, 10 mM HEPES, pH 7.4. The current signals were filtered at 10 kHz and sampled at 50 kHz.

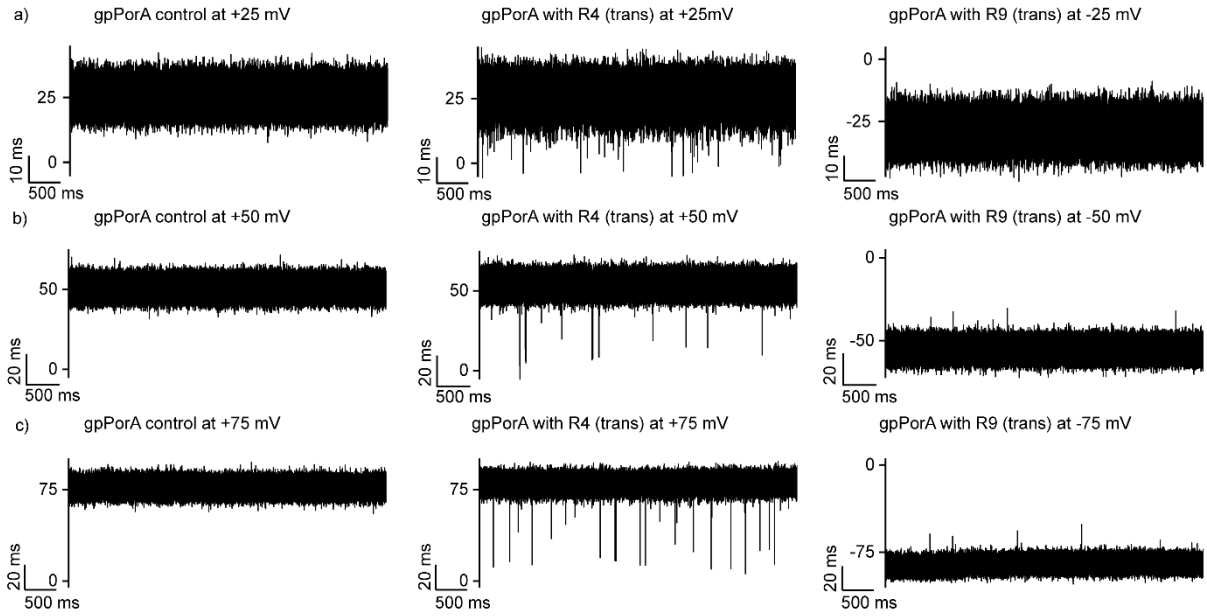

Fig. S5: Interaction of tetraarginine with the gpPorA

a) Electrical recordings showing gpPorA at +25 mV and the interaction of tetraarginine (R4) with single gpPorA (10 µM, trans) at ±25. **b)** Electrical recordings showing gpPorA at +50 mV the interaction of R4 with single gpPorA (10 µM, trans) at ± 50 mV **c)** Electrical recordings showing gpPorA at +75 mV and the interaction of R4 with single gpPorA (10 µM, trans) at ±75. Electrolyte: 150 mM KCl, 10 mM HEPES, pH 7.4. The current signals were filtered at 10 kHz and sampled at 50 kHz.

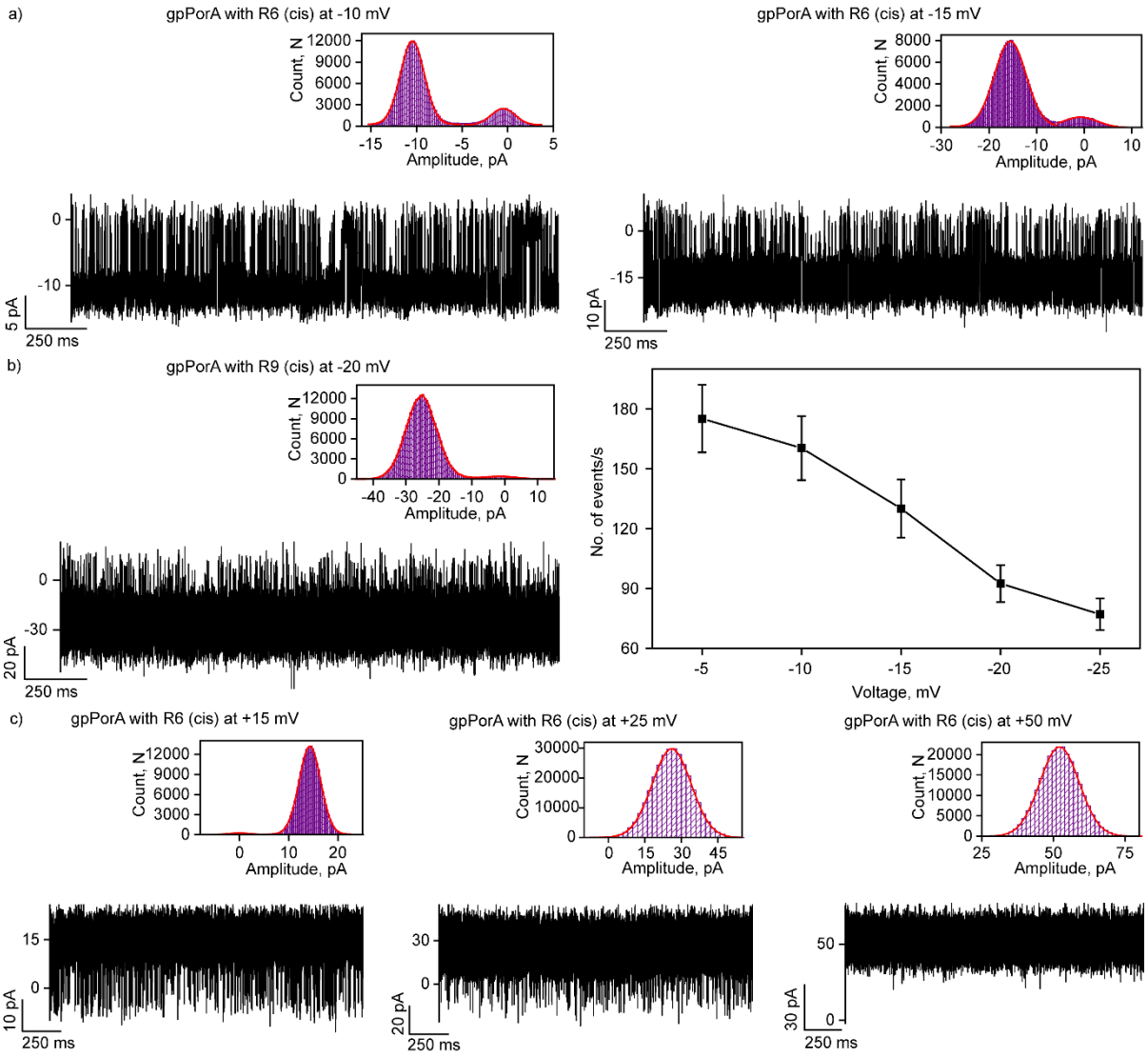

Fig. S6: Interaction of hexaaarginine with the cis side of the gpPorA

a) Electrical recordings showing the interaction of hexaarginine (R6) with single gpPorA (0.5 µM, cis) at -10 mV and -15 mV. **b)** Electrical recordings showing the interaction of R6 with single pPorA (0.5 µM, cis) at -20 mV and a plot of number of events/s versus the applied voltage. (Mean values (±s.d.) from three independent experiments are shown). **c)** Electrical recordings showing the interaction of R6 with single gpPorA (0.5 µM, cis) at +15 mV and + 25 mV and + 50 mV against electrophoretic mobility. The current amplitude histogram is shown. Electrolyte: 150 mM KCl, 10 mM HEPES, pH 7.4. The current signals **a)** -10 mV, -15 mV and **b)** -20 mV were digitally filtered at 2 kHz, 4 kHz and 5 kHz using an 8-pole Bessel digital filter. The current signals **c)** +15 mV, +25 mV and +50 mV were digitally filtered at 3 kHz and 10 kHz using an 8-pole Bessel digital filter.

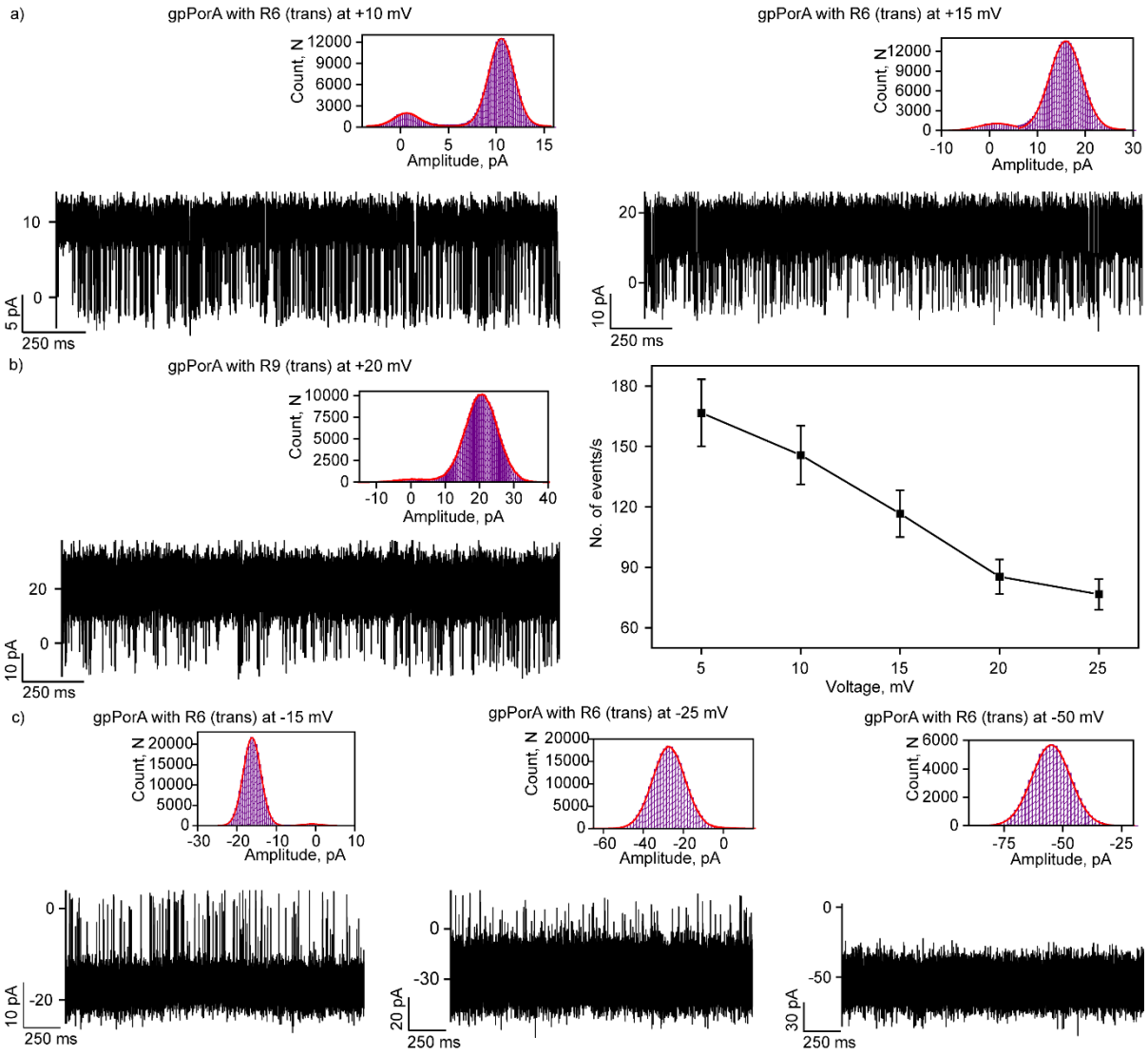

Fig. S7: Interaction of hexaaarginine with the trans side of the gpPorA

a) Electrical recordings showing the interaction of R6 with single gpPorA (0.5 µM, trans) at +10 mV and +15 mV **b)** Electrical recordings showing the interaction of R6 with single gpPorA (0.5 µM, trans) at +20 mV and a plot of the number of events /s versus the applied positive potential. **c)** Electrical recordings showing the interaction of R6 with single gpPorA (0.5 µM, trans) at -15 mV, -25 mV and -50 mV against electrophoretic mobility. The corresponding amplitude histogram is shown. Electrolyte: 150 mM KCl, 10 mM HEPES, pH 7.4. The current signals **a)** +10 mV, +15 mV and **b)** +20 mV were digitally filtered at 2 kHz, 4 kHz and 5 kHz using an 8-pole Bessel digital filter. The current signals **c)** -15 mV, -25 mV and -50 mV were digitally filtered at 3 kHz and 10 kHz using an 8-pole Bessel digital filter.

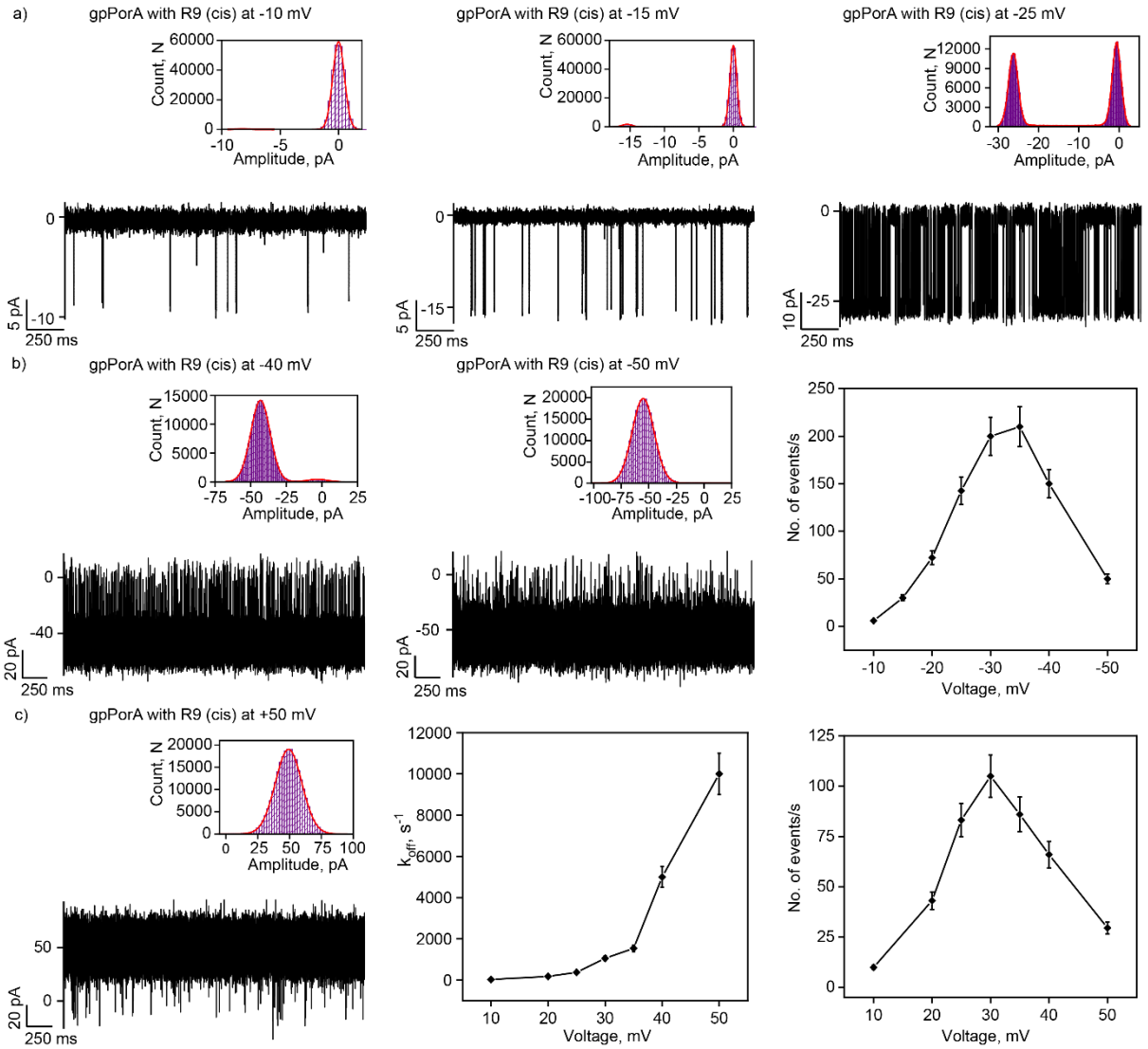

Fig. S8: Interaction of nonaarginine with the cis side of the gpPorA

a) Electrical recordings showing the interaction of nonaarginine (R9) with single gpPorA (0.5 µM, cis) at -10 mV, -15 mV and -25 mV **b)** at -40mV, -50 mV and a plot of number of events/s versus applied negative voltages. **c)** Electrical recordings showing the interaction of R9 with single gpPorA (0.5 µM, cis) at +50 mV, a plot of k_{off} and the number of release events/s versus the applied positive voltages. (Mean values (±s.d.) from three independent experiments are shown). The corresponding current amplitude histogram is shown. Electrolyte: 150 mM KCl, 10 mM HEPES, pH 7.4. The current signals **(a)** -10 mV, -15 mV were digitally filtered at 1 kHz and -25 mV at 2 kHz using an 8-pole Bessel digital filter, **(b)** -40 mV and -50 mV were digitally filtered at 7 kHz and 10 kHz using an 8-pole Bessel digital filter and **(c)** +50 mV were digitally filtered at 10 kHz using an 8-pole Bessel digital filter.

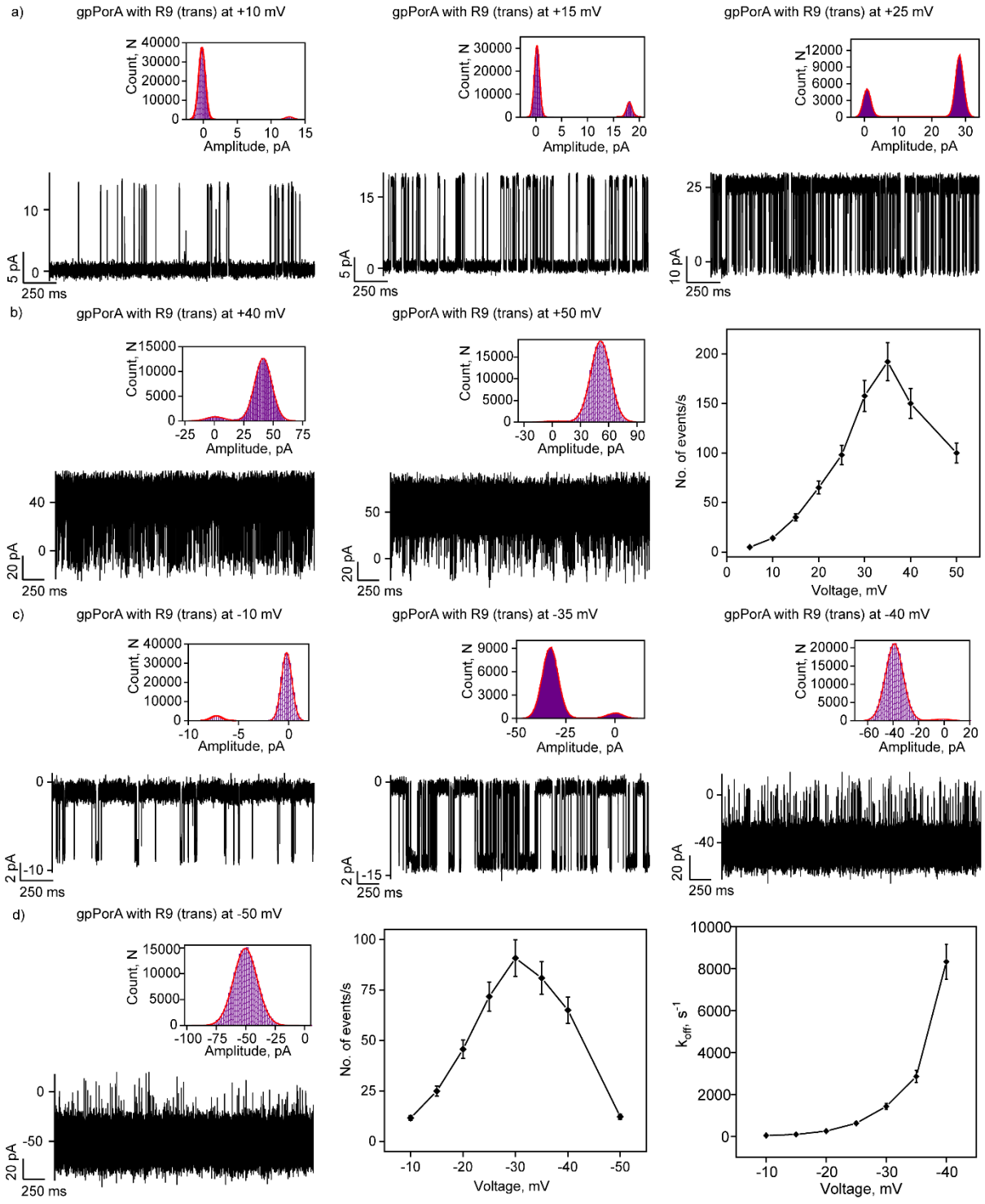

Fig. S9: Interaction of nonaarginine with trans side of the gpPorA

a) Electrical recordings showing interaction of R9 with single gpPorA (0.5 µM, trans) at +10 mV, +15 mV and +25 mV. **b)** at +40 mV, +50 mV and a plot of number of events/s versus applied positive voltages **c)** R9 with single gpPorA (0.5 µM, trans) at -10 mV, -35 mV and -40 mV. **d)** R9 with single pPorA (0.5 µM, trans) at -50 mV, and a plot of the number of release events/s and k_{off} versus the applied negative voltages. (Mean values (±s.d.) from three

independent experiments are shown). The corresponding amplitude histogram is shown. Electrolyte: 150 mM KCl, 10 mM HEPES, pH 7.4. The current signals **(a)** +10 mV, +15 mV were digitally filtered at 1 kHz and +25 mV at 2 kHz using an 8-pole Bessel digital filter, **(b)** +40 mV and +50 mV were digitally filtered at 7 kHz and 10 kHz using an 8-pole Bessel digital filter, **(c, d)** -10, -15 mV was digitally filtered at 1 kHz, and -40 mV and -50 mV were digitally filtered at 7 kHz and 10 kHz using an 8-pole Bessel digital filter.

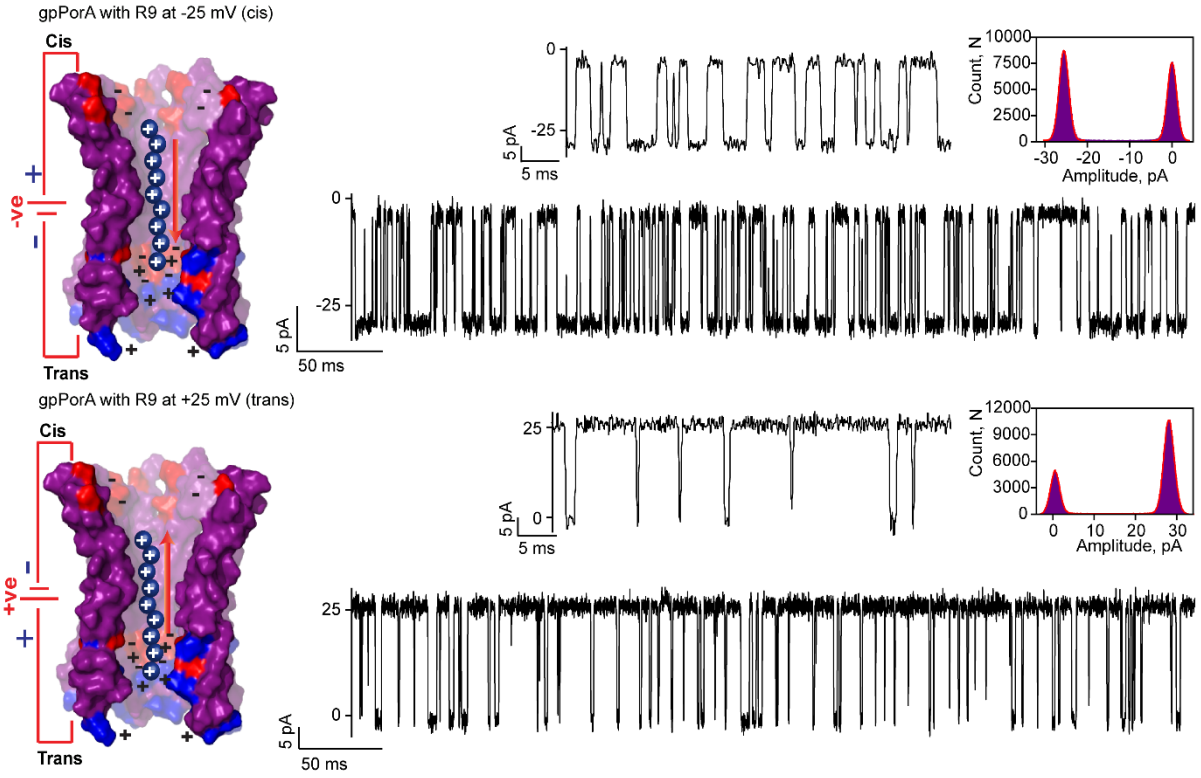

Fig. S10: The interaction of nonaarginine with the cis and trans side of the gpPorA. Electrical recordings showing the interaction of R9 with the cis and trans side of single gpPorA (0.5 µM) at ± 25 mV. The model showing the interaction of R9 with the cis and trans side of the pore is shown. Electrolyte:150 mM KCl, 10 mM HEPES, pH 7.4. The current signals ±25 mV were digitally filtered at 2 kHz using an 8-pole Bessel digital filter.

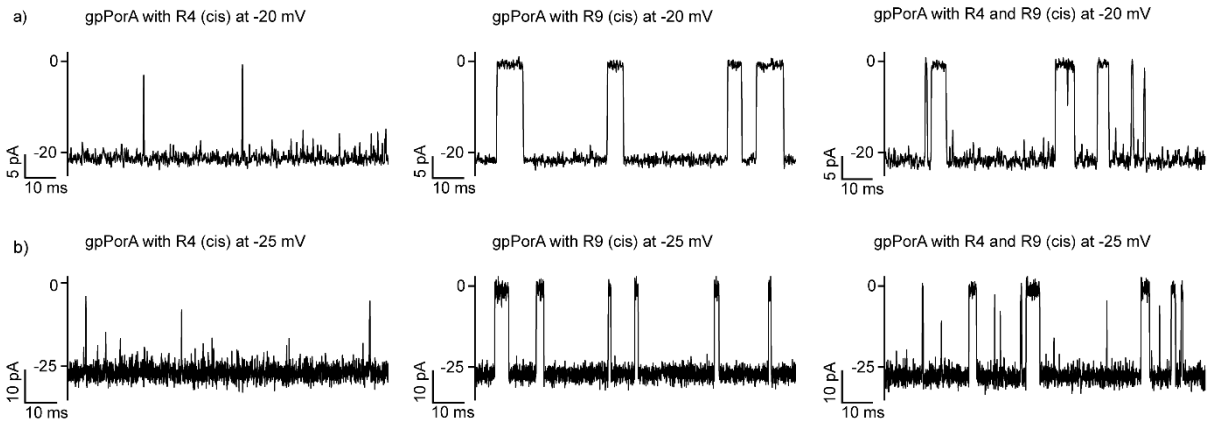

Fig. S11: Interaction of tetraarginine and nonaarginine with gpPorA

a) Competitive interaction of the gpPorA with R4 (10 µM, cis) and R9 (both 100 nM, cis) at -20 mV and **b)** -25 mV. Electrolyte:150 mM KCl, 10 mM HEPES, pH 7.4. The current signals **(a, b)** were filtered at 2 kHz and 5 kHz using an 8-pole Bessel digital filter.

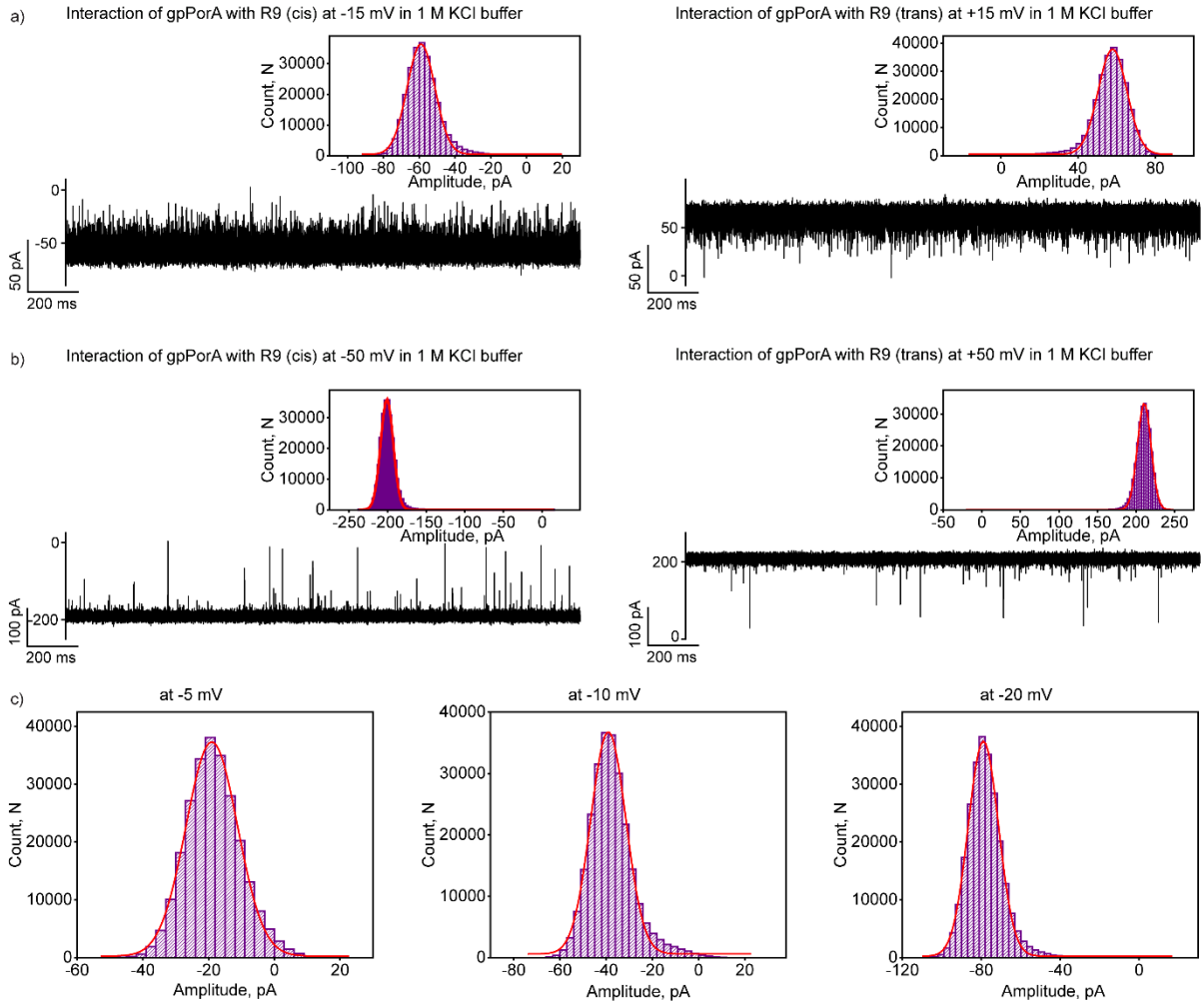

Fig. S12: Interaction of nonaaarginine with gpPorA in 1 M KCl buffer

a) Electrical recordings showing the interaction of nonaarginine (R9) with single gpPorA (100 µM, cis) at -15 mV and (100 µM, trans) at +15 mV. **b)** Electrical recordings showing the interaction of R9 with single gpPorA (100 µM, cis) at -50 mV and (100 µM, trans) at +50 mV. The corresponding amplitude histogram is shown. **c)** The amplitude histogram is shown for voltages -5 mV, -10 mV and -20 mV (R9, 100 µM cis). Electrolyte: 1 M KCl, 10 mM HEPES, pH 7.4. The current signals were filtered at 10 kHz and sampled at 50 kHz.

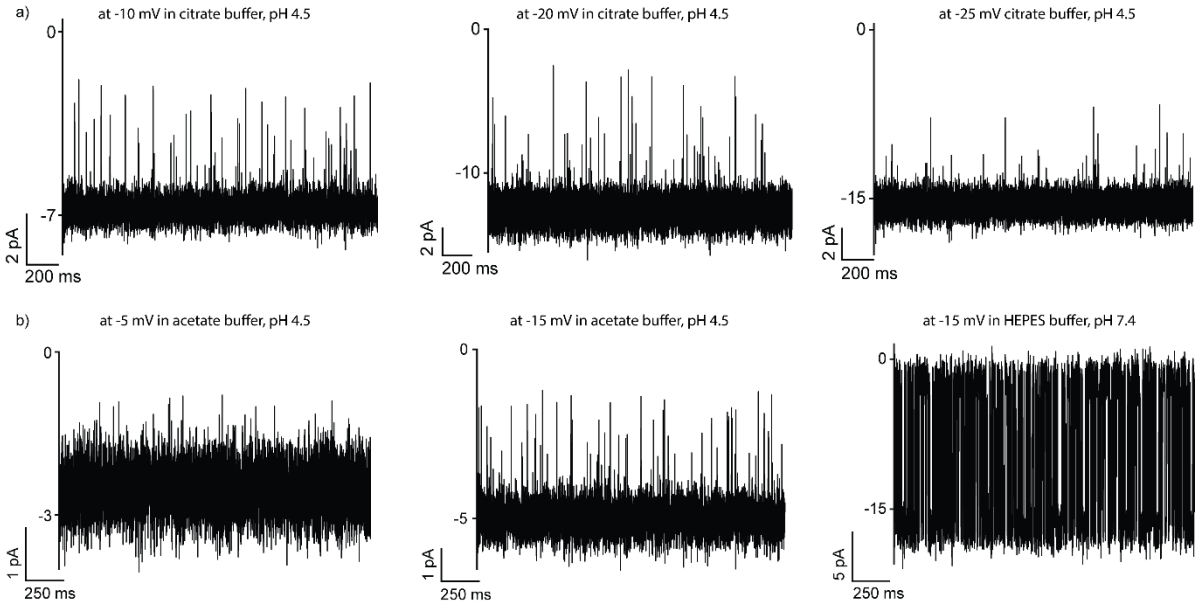

Fig. S13: pH-dependent interaction of nonaarginine with gpPorA

a) Electrical recordings showing the interaction of R9 with single gpPorA (0.5 µM, cis) at -10 mV, -20 mV and -25 mV. 0.15 M KCl, citrate buffer, pH 4.5. **b)** Electrical recordings showing the interaction of R9 with single gpPorA (0.5 µM, cis) at -5 mV, -15 mV pH 4.5 and -15 mV 0.15 M KCl, 10 mM HEPES, pH 7.4 and acetate buffer, pH 4.5. The current signals were digitally filtered at 1kHz using an 8-pole Bessel digital filter, respectively.

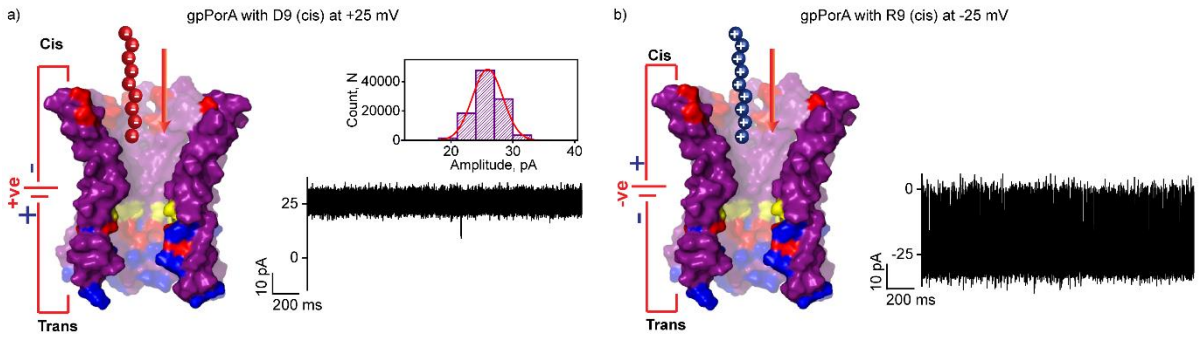

Fig. S14: Interaction of nonaspartate and nonaarginine with gpPorA

a) Electrical recordings showing the interaction of D9 with the cis side of single gpPorA (100 µM) at + 25 mV **b)** Electrical recordings showing the interaction of R9 with the cis side of same single gpPorA (0.5 µM) at - 25 mV. Electrolyte:150 mM KCl, 10 mM HEPES, pH 7.4. The current signals **(a)** +25 mV were digitally filtered at 2 kHz using an 8-pole digital filter **(b)** -25 mV was filtered at 10 kHz and sampled at 50 kHz.

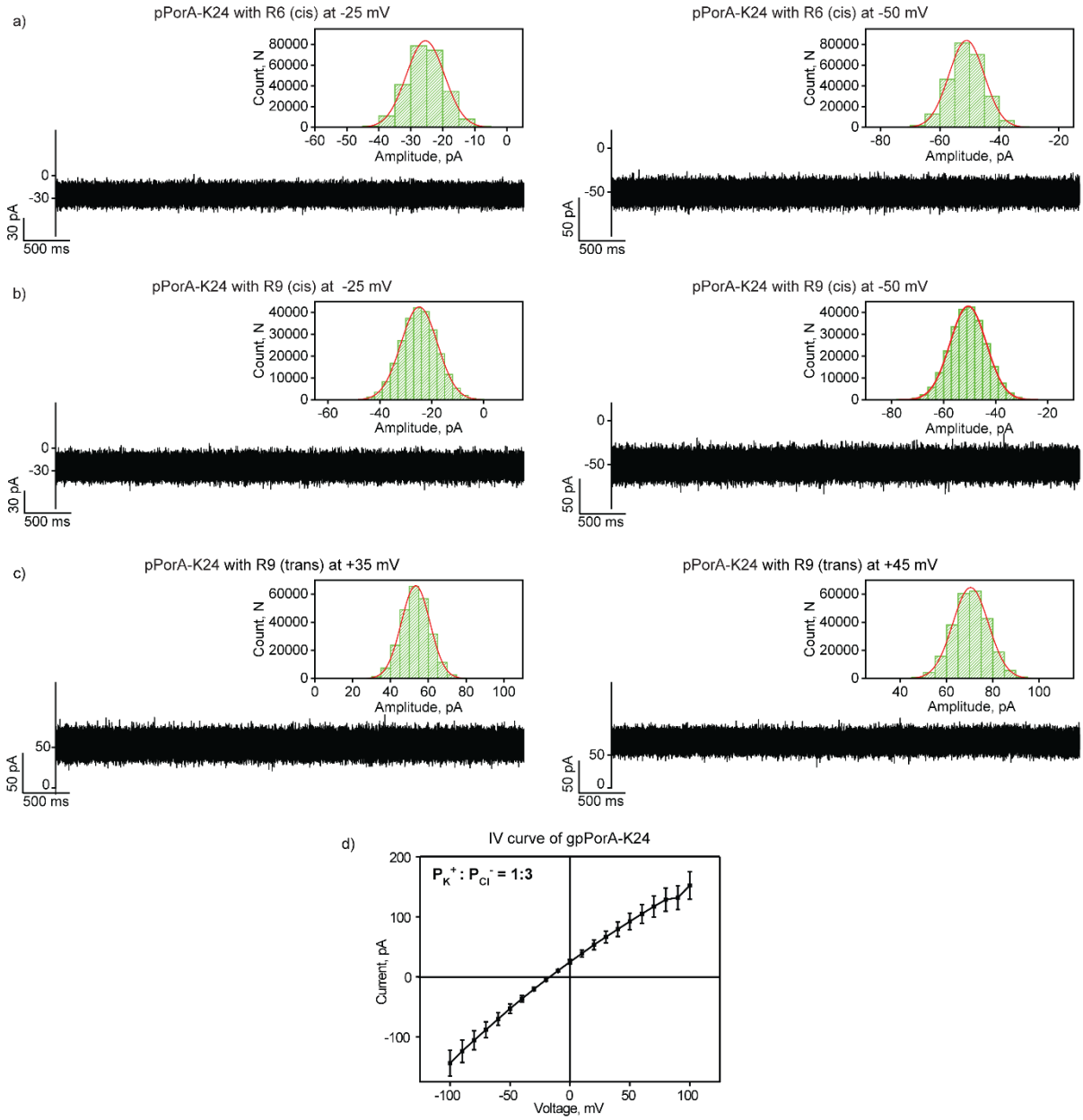

Fig. S15: Interaction of hexaarginine and nonaarginine with pPorA-K24.

a) Electrical recordings showing the interaction of hexaarginine (R6) with pPorA- K24 (50 µM, cis) at -25 mV and -50 mV **b)** Electrical recordings showing the interaction of nonaarginine (R9) with pPorA-K24 (25 µM, cis) at -25 mV and -50 mV. **c)** Electrical recording showing the interaction of nonaarginine (R9) with pPorA-K24 (25 µM, trans) at +35 mV and +45 mV. **d)** Reverse potential obtained from the I-V curve of a single pPorA-K24. Electrolyte: 150 mM KCl, 10 mM HEPES, pH 7.4. The current signals were filtered at 10 kHz and sampled at 50 kHz.

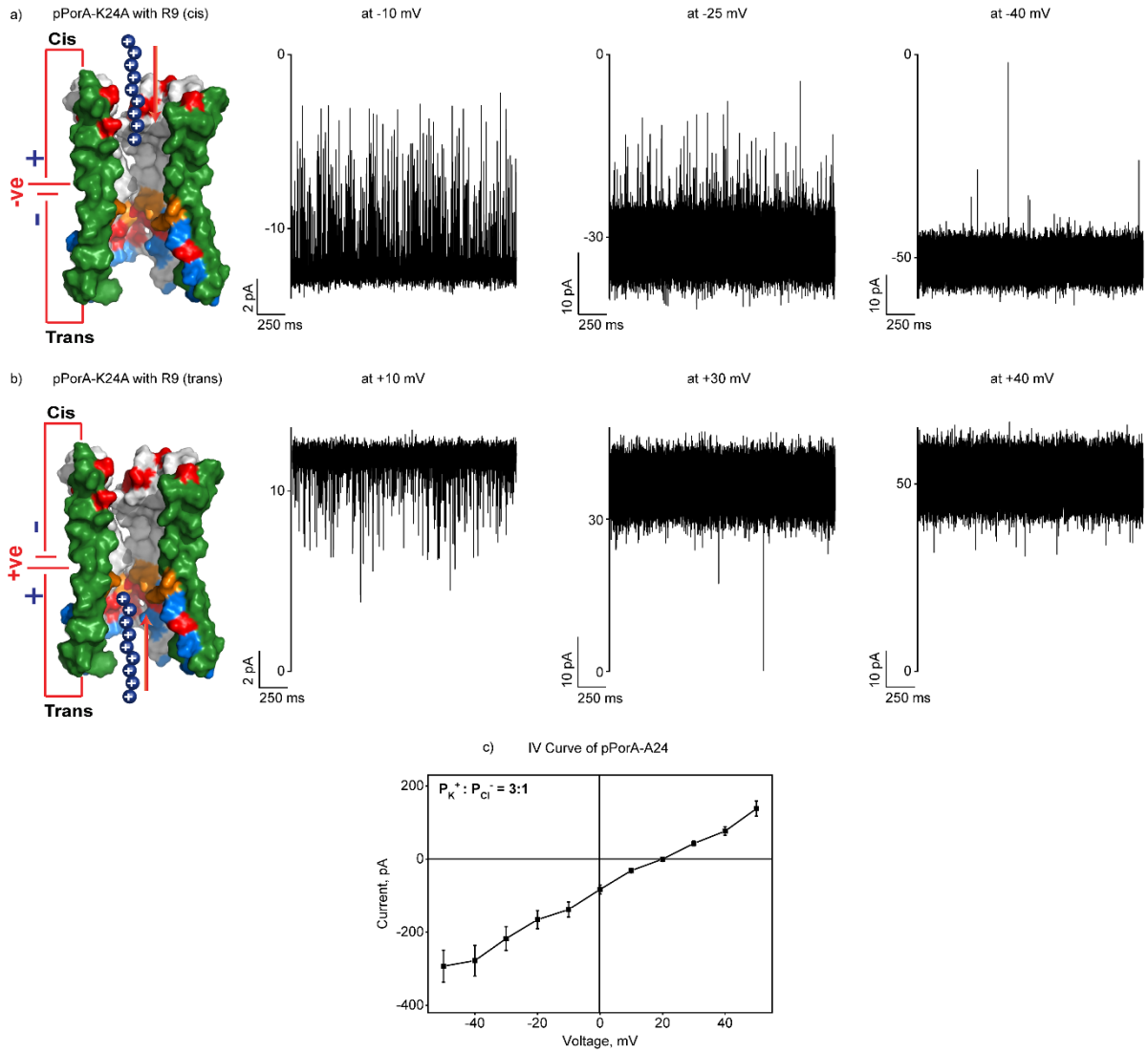

Fig. S16: Interaction of nonaarginine with pPorA-A24.

a) Electrical recordings showing the interaction of R9 with single pPorA-A24 (0.5 µM, cis) at -10 mV, -25 mV and -40 mV. **b)** Electrical recordings showing the interaction of R9 with single pPorA-A24 (0.5 µM, trans) at +10 mV, +30 mV and +40 mV. Model showing the interaction of R9 with the cis and trans side of the pore. **c)** Reverse potential obtained from the I-V curve of a single pPorA-K24. Electrolyte: 150 mM KCl, 10 mM HEPES, pH 7.4. The current signals **(a)** -10 mV, -25 mV and -40 mV were digitally filtered at 1 kHz, and 7 kHz. The current signals **(b)** +10 mV, +30 mV and +40 mV were digitally filtered at 1 kHz and 7 kHz using an 8-pole Bessel digital filter.

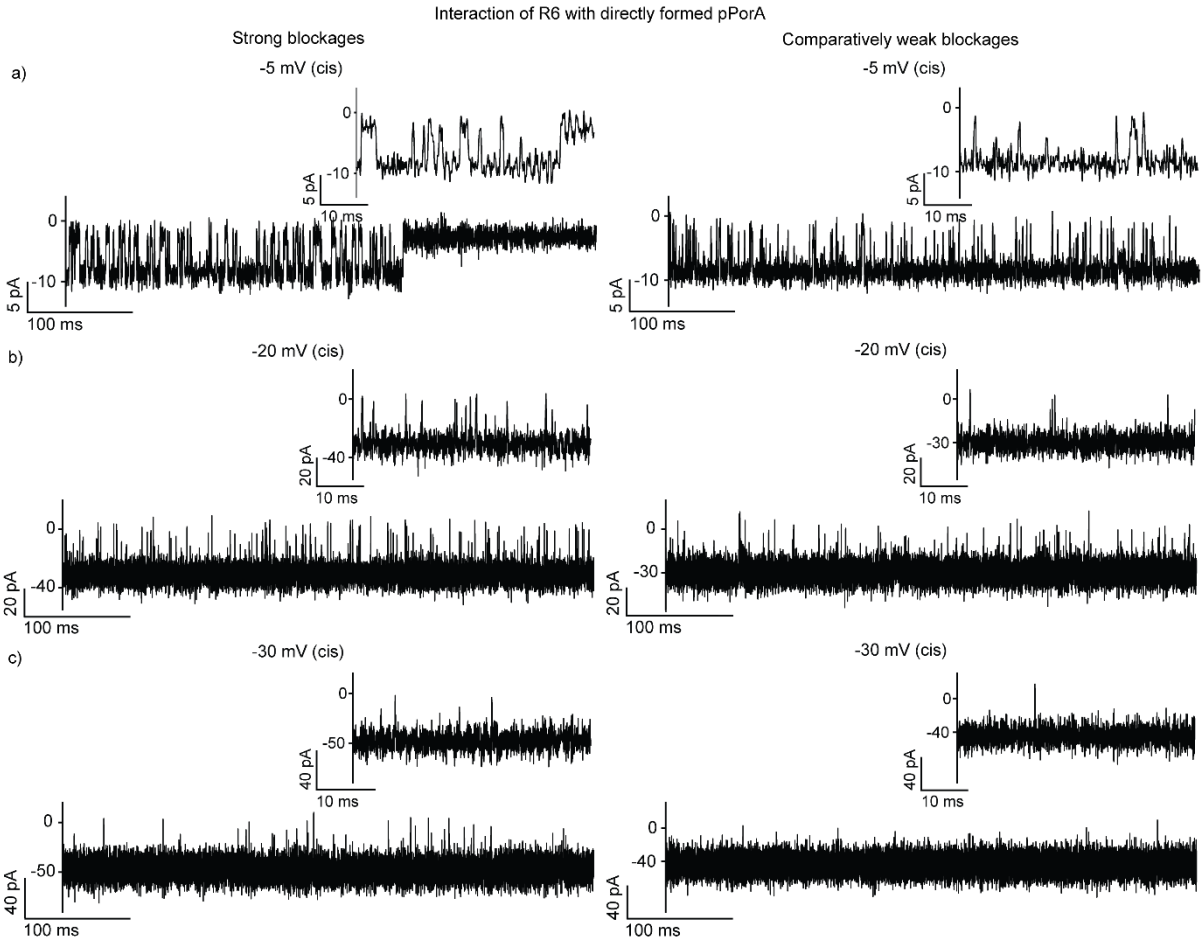

Fig. S17: Interaction of cationic hexaarginine with directly added pPorA peptides.

Electrical recordings showing strong and comparatively weak interaction of hexaarginine with single pPorA (1 µM, cis) at **a)** -5 mV, **b)** -20 mV and **c)** -30 mV. Electrolyte: 150 mM KCl, 10 mM HEPES, pH 7.4. The current signals **(a)** were digitally filtered at 1.5 kHz, **(b)** were digitally filtered at 5 kHz and **(c)** were digitally filtered at 7 kHz using an 8-pole Bessel digital filter.

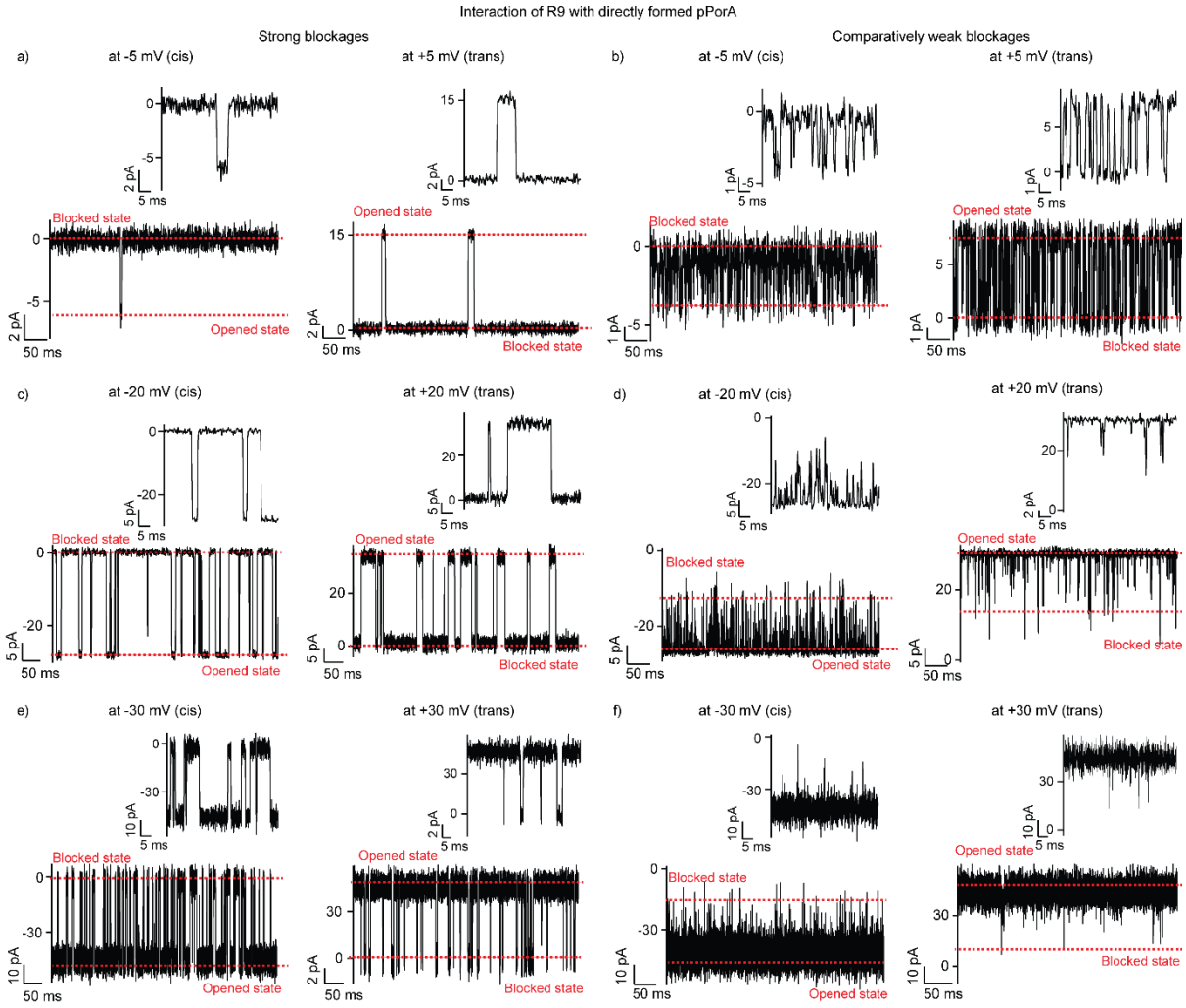

Fig. S18: Interaction of cationic nonaarginine with directly added pPorA peptides. **a)** Electrical recordings showing strong interaction of nonaarginine with single pPorA (0.5 µM, trans) at -5 mV (cis) and +5 mV (trans) **b)** Electrical recordings comparatively weak interaction of nonaarginine with single pPorA (0.5 µM, trans) at -5 mV (cis) and +5 mV (trans) **c)** Electrical recordings showing the strong interaction of nonaarginine with single pPorA (0.5 µM, trans) at -20 mV (cis) and +20 mV (trans) **d)** Electrical recordings showing comparatively weak interaction of nonaarginine with single pPorA (0.5 µM, trans) at -20 mV (cis) and +20 mV (trans). **e)** Electrical recordings showing the strong interaction of nonaarginine with single pPorA (0.5 µM, trans) at -30 mV (cis) and +30 mV (trans) **f)** Electrical recordings showing comparatively weak interaction of nonaarginine with single pPorA (0.5 µM, trans) at -30 mV (cis) and +30 mV (trans). The current signals **(a), (b)** -5 mV and +5 mV were digitally filtered at 1 kHz. **(c), (d)** -20 mV was digitally filtered at 1 kHz and +20 mV was digitally filtered at 2 kHz **(e), (f)** -30 mV and 30 mV were digitally filtered at 5 kHz using an 8-pole Bessel digital filter.

References:

1. N. Abdali, E. Barth, A. Norouzy, R. Schulz, W. M. Nau, U. Kleinekathofer, A. Tauch and R. Benz, *PLoS One*, 2013, **8**, e75651.

2. R. S. Krishnan, R. Satheesan, N. Puthumadathil, K. S. Kumar, P. Jayasree and K. R. Mahendran, *J. Am. Chem. Soc.*, 2019, **141**, 2949-2959.

3. J. Lee, X. Cheng, J. M. Swails, M. S. Yeom, P. K. Eastman, J. A. Lemkul, S. Wei, J. Buckner, J. C. Jeong, Y. Qi, S. Jo, V. S. Pande, D. A. Case, C. L. Brooks, 3rd, A. D. MacKerell, Jr., J. B. Klauda and W. Im, *J. Chem. Theory Comput.*, 2016, **12**, 405-413.

4. K. Vanommeslaeghe, E. Hatcher, C. Acharya, S. Kundu, S. Zhong, J. Shim, E. Darian, O. Guvench, P. Lopes, I. Vorobyov and A. D. Mackerell, Jr., *J. Comput. Chem.*, 2010, **31**, 671 690.

5. J. C. Phillips, R. Braun, W. Wang, J. Gumbart, E. Tajkhorshid, E. Villa, C. Chipot, R. D. Skeel, L. Kale and K. Schulten, *J. Comput. Chem.*, 2005, **26**, 1781-1802.

6. Y. Miao, V. A. Feher and J. A. McCammon, *J. Chem. Theory Comput.*, 2015, **11**, 3584-3595.

7. K. R. Mahendran, A. Niitsu, L. Kong, A. R. Thomson, R. B. Sessions, D. N. Woolfson and H. Bayley, *Nat. Chem.*, 2017, **9**, 411-419.